Order−Disorder Phenomena in New $LaBaMn_2O_{6-x}$ CMR Perovskites. Crystal and Magnetic Structure

F. Millange,* V. Caignaert, B. Domengès, and B. Raveau

Laboratoire CRISMAT, ISMRA, Université de Caen, 6 Boulevard du Maréchal Juin, 14050 CAEN Cedex, France

E. Suard

Institut Laue-Langevin, 38042 GRENOBLE Cedex 9, France

Received March 4, 1998. Revised Manuscript Received April 27, 1998

Three new perovskites in the $LaBaMn_2O_{6-x}$ family have been synthesized by controlling the oxygen pressure, during both synthesis and postannealing. Structural determination from powder neutron diffraction (PND) data shows that one form of $LaBaMn_2O_6$ is cubic (a = 3.906 Å), with a disordered distribution of La^{3+} and Ba^{2+} cations, whereas a second form of $LaBaMn_2O_6$ is tetragonal (a = 3.916 Å; c = 7.805 Å), with an alternate stacking of lanthanum and barium layers along c. The same La/Ba cation order is observed for the ordered, oxygen-deficient perovskite $LaBaMn_2O_5$, which is also tetragonal (a = 5.650 Å; c = 7.808 Å) and adopts a $YBaCuFeO_5$-related structure. Elucidation of the magnetic structure of $LaBaMn_2O_5$, from low-temperature PND data, leads to a G-type antiferromagnetic model; the superimposed Mn^{2+}/Mn^{3+} charge order results in ferrimagnetic behavior for this phase and explains its magnetic properties, as obtained from susceptibility measurements. In both forms of $LaBaMn_2O_6$, the PND data show a ferromagnetic contribution. The CMR properties of the "O_6" forms exhibit a remarkable feature: T_C is increased from 270 K for the disordered phase to 335 K for the ordered one, probably owing to the La/Ba ordering.

1. Introduction

Among the numerous manganese oxides with colossal magnetoresistance (CMR) properties, the manganites $La_{1-y}Ba_yMnO_3$ offer a particular interest in that they exhibit large resistance ratios above room temperature. Several perovskite-based phases have been isolated for the lanthanum-rich compositions $La_{1-y}Ba_yMnO_3$, y < 0.4.[1−5] For instance, bulk of $La_{0.65}Ba_{0.35}MnO_3$ has a T_C of 362 K.[5] Such high T_C's are a result of the relatively large average size of the A-site cation, since it has been shown that T_C increases as $\langle r_A \rangle$ increases.[6,7] However, there exists an antagonist effect, called "mismatch", owing to the size difference between the A-site cations (La and Ba) which opposes the increase of T_C.[8] The latter effect results from local lattice distortions due to the disorder of the A-site cations. These observations suggest that it should be possible to suppress the mismatch effect in the perovskites $La_{1-y}Ba_yMnO_3$ by inducing an ordering between the La^{3+} and Ba^{2+} cations. While several perovskite-based phases have been isolated for the lanthanum-rich compositions $La_{1-y}Ba_yMnO_3$, the perovskite $La_{0.5}Ba_{0.5}MnO_3$ has never been synthesized owing to the formation of the hexagonal related perovskite $BaMnO_{3-\epsilon}$[9,10] for x > 0.4. Recently, through the use of a two-step synthesis method, the composition corresponding to x = 0.5 has been investigated. The cubic perovskite $La_{0.5}Ba_{0.5}MnO_3$ is of great interest, although it exhibits a T_C of only 270 K. For this manganite, which will be formulated as $LaBaMn_2O_6$ herein, we have considered the possibility of ordering the La^{3+} and Ba^{2+} cations in the form of layers, as in the oxygen-deficient perovskite $YBaCuFeO_5$[11,12] or $YBaMn_2O_5$.[13] For this purpose, we successfully synthesized the ordered, oxygen-deficient perovskite $LaBaMn_2O_5$ and then, in a second step, we obtained the ordered, stoichiometric perovskite $LaBaMn_2O_6$ by annealing at low temperature in an oxygen

* Corresponding author. E-mail: millange@crismat.ismra.fr.

(1) Von Helmolt, R.; Wecker, J.; Holzapfel, B.; Schultz, L.; Sammer, K. *Phys. Rev. Lett.* **1993**, *71*, 2331.
(2) Xiong, G. C.; Li, Q.; Ju, H. L.; Greene, R. L.; Venkatesan, T. *Appl. Phys. Lett.* **1995**, *66*, 13.
(3) Ju, H. L.; Gopalakrishnan, J.; Peng, J. L.; Xiong, G. C.; Venkatesan, T.; Greene, R. L. *Phys. Rev. B* **1996**, *51*, 6143.
(4) Radaelli, P. G.; Marezio, M.; Hwang, H. Y.; Cheong, S. W. *J. Solid State Chem.* **1996**, *122*, 444.
(5) Barnabe, A.; Millange, F.; Maignan, A.; Hervieu, M.; Raveau, B.; Van Tendeloo, G.; Raveau, B. *Chem. Mater.* **1998**, *10*, 252.
(6) Millange, F.; Maignan, A.; Caignaert, V.; Simon, Ch.; Raveau, B. *Z. Phys. B* **1996**, *101*, 169−174.
(7) Maignan, A.; Simon, Ch.; Caignaert, V.; Hervieu, M.; Raveau, B. *Z. Phys. B* **1996**, *99*, 305.
(8) Rodriguez-Martinez, L. M.; Attfield, J. P. *Phys. Rev. B* **1996**, *54*, 22.
(9) Jonker, G. H.; Van Santen, J. H. *Physica* **1950**, *16*, 337.
(10) Negas, T.; Roth, R. S. *J. Solid State Chem.* **1971**, *3*, 323.
(11) Er-Rakho, L.; Michel, C.; Lacorre, P.; Raveau, B. *J. Solid State Chem.* **1988**, *73*, 531.
(12) Caignaert, V.; Mirebeau, I.; Bourée, F.; Nguyen, N.; Ducouret, A.; Greneche, J. M.; Raveau, B. *J. Solid State Chem.* **1995**, *114*, 24.
(13) Chapman, J. P.; Attfield, J. P.; Molgg, M.; Friend, C. M.; Beales, T. P. *Angew. Chem., Int. Ed. Engl.* **1996**, *35*, 2482.
(14) Rodriguez-Carvajal, J. In *Satellite Meeting on Powder Diffraction*, Abstracts of the XVth Conference of the International Union of Crystallography, Toulouse, 1990, p 127.
(15) Sears, V. F. Chalk River Nuclear Laboratory Internal Report AECL-8490, 1984.

S0897-4756(98)00130-6 CCC: $15.00
Published on Web 06/20/1998

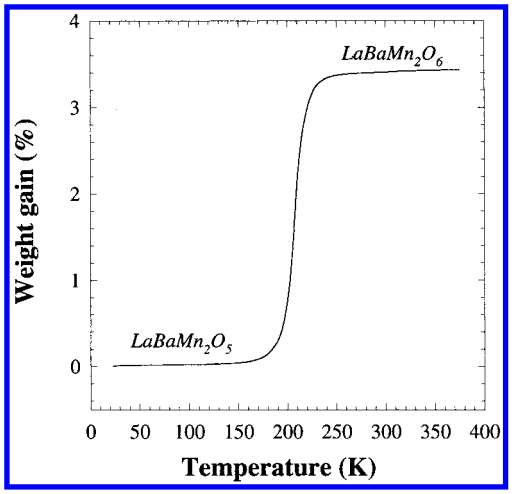

Figure 1. TG weight gain versus temperature under an oxidizing atmosphere (O_2) for the ordered, oxygen-deficient perovskite $LaBaMn_2O_5$.

flow. Attfield et al.[13] have reported that $YBaMn_2O_5$ decomposes irreversibly into $YMnO_3$ and $BaMnO_3$ above 220 °C in air or oxygen. In the present paper, we report on the synthesis and the crystal and magnetic structures of two stoichiometric perovskites, $LaBaMn_2O_6$ (ordered and disordered), and the ordered, oxygen-deficient perovskite $LaBaMn_2O_5$.

2. Experimental Section

The purity of the samples (whose synthesis is described in 3.1 below) was first verified from X-ray diffraction data registered with a Philips diffractometer using Cu Kα radiation. The ordered-phase $LaBaMn_2O_5$ was subsequently registered on the D1a high-resolution neutron powder diffractometer at Institut Laue-Langevin with a wavelength of 1.907 Å at three temperatures: 1.7 and 70 K and room temperature. The sample was contained in a vanadium can. The high-flux powder diffractometer D1b was used to investigate the thermal dependence of the magnetic structure in the temperature range of 70−100 K. The ordered form of the stoichiometric phase $LaBaMn_2O_6$ was registered on D1a at 1.7 and 400 K and room temperature, while the cubic form of $LaBaMn_2O_6$ was registered on the high-resolution diffractometer D2b using a wavelength of 1.594 Å. The nuclear and magnetic refinements were performed using the profile fitting program Fullprof[14] ($b_{La} = 0.824 \times 10^{-12}$ cm; $b_{Ba} = 0.525 \times 10^{-12}$ cm; $b_{Mn} = -0.373 \times 10^{-12}$ cm; $b_O = 0.58 \times 10^{-12}$ cm).[15]

Samples for electron microscopy were crushed in n-butanol, and the microcrystals were deposited on a holey carbon-coated film (copper grid). The electron diffraction (ED) study was carried out with a JEM 200CX fitted with a tilting−rotating sample holder (±60°). The high-resolution electron microscopy (HREM) and the convergent beam electron diffraction (CBED) studies were performed with a TOPCON 002B microscope having a point resolution of 1.8 Å. Both microscopes were equipped with EDS, which allows confirmation of the cationic composition and the homogeneity within the crystals.

Magnetization measurements were made with a SQUID (MPMS Quantum Design) magnetometer. These DC susceptibility measurements were carried out at low field (100 G) with increasing temperature after the samples were either zero field cooled (ZFC) or field cooled (FC).

AC susceptibilities were measured with a Lake Shore 7000 susceptometer ($8 \le f \le 666$ Hz; $5 \le T \le 320$ K; $10^{-2} \le h_{AC} \le 10$ G).

Resistivities were measured between 5 and 400 K, on bars with the approximate dimensions of $0.2 \times 0.2 \times 1$ cm^3, using a standard four-points method. Magnetoresistance measurements were performed using applied magnetic fields up to 7 T, with temperatures ranging from 5 to 400 K.

The thermogravimetric (TG) analysis was realized with a Setaram microbalance under an oxygen flow.

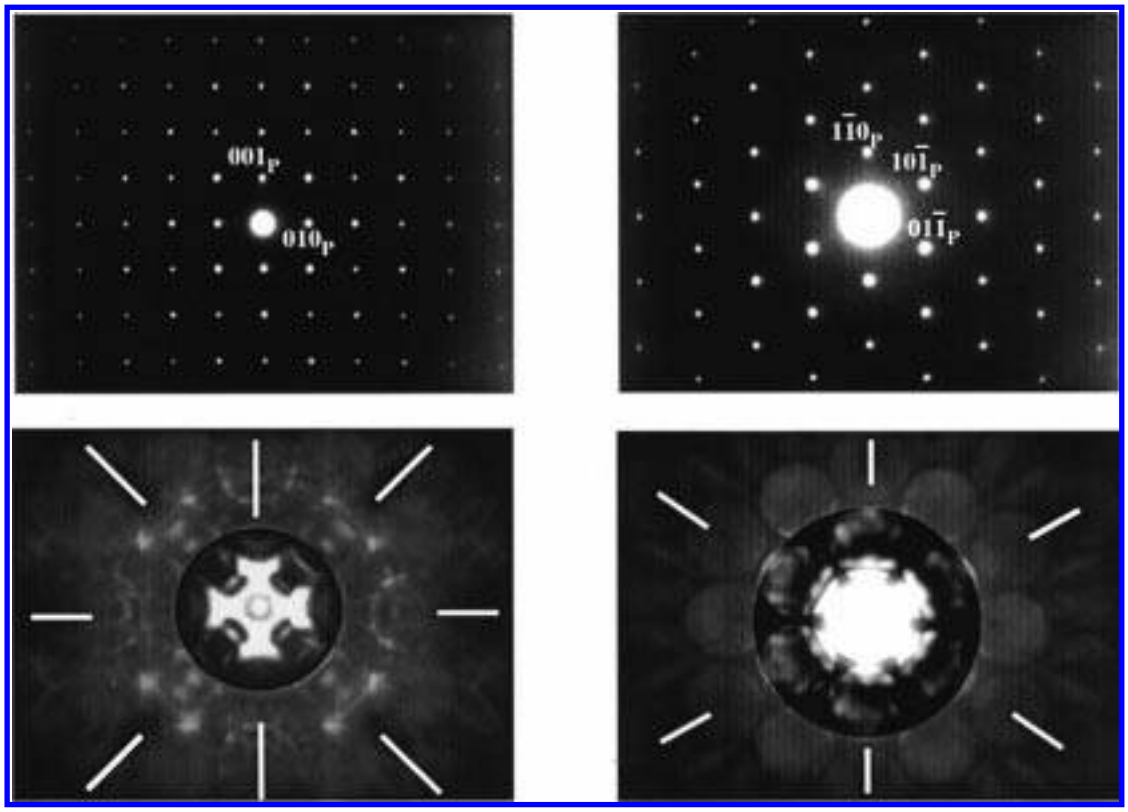

Figure 2. [100] and [111] SAED and CBED patterns index to an $a_p \times a_p \times a_p$ cell and are in agreement with a $Pm3m$ space group.

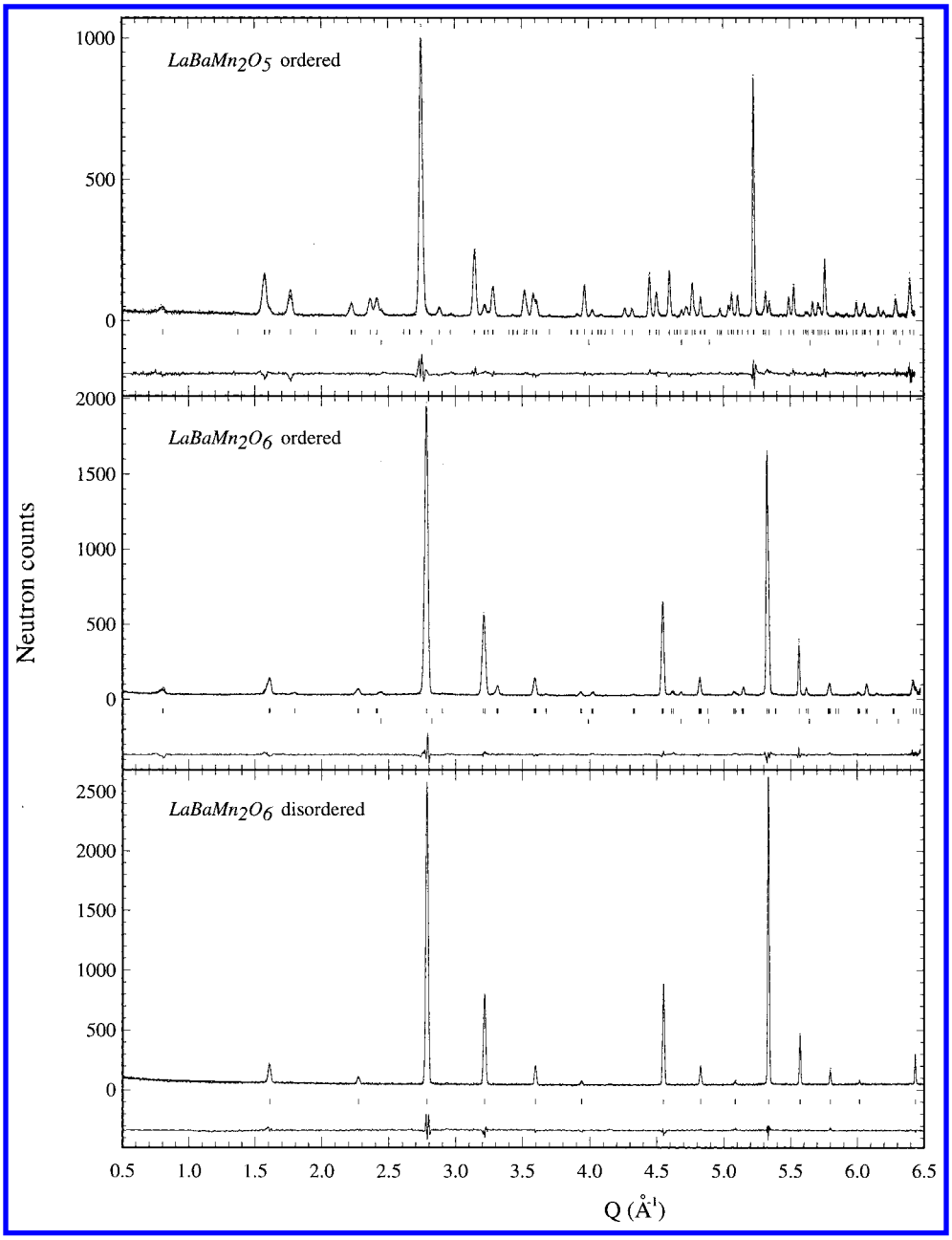

Figure 3. Rietveld refinement plot of the neutron diffraction data. The ticks are given for nuclear structure peaks (top row) and MnO impurity nuclear peaks (bottom row). Top: Ordered $LaBaMn_2O_5$ at room temperature. Middle: Ordered $LaBaMn_2O_6$ at T = 400 K. Bottom: Disordered $LaBaMn_2O_6$ at room temperature.

3. Results and Discussion

3.1. Synthesis of Three New Perovskites: $LaBaMn_2O_6$ (Ordered and Disordered) and $LaBaMn_2O_5$ (Ordered)

The synthesis of the perovskites $LaBaMn_2O_6$ and $LaBaMn_2O_5$ is partially hindered by the formation of the hexagonal related perovskite $BaMnO_{3-\epsilon}$.[10] To avoid the formation of the latter, both the partial oxygen pressure and the temperature had to be carefully controlled during the synthesis.

The disordered cubic perovskite $LaBaMn_2O_6$ was prepared by reacting appropriate mixtures of La_2O_3, MnO_2, and $BaCO_3$. The reagent powders were ground and calcined in a mixed Ar/O_2 flow at 1500 °C to avoid the complete oxidization of Mn^{3+} to Mn^{4+}, which would favor the formation of $BaMnO_{3-\epsilon}$. The products were cooled to 800 °C in the same atmosphere and finally cooled slowly to room temperature in an oxidizing atmosphere (O_2) to optimize the oxygen content of the sample. When the products are oxidized below 800 °C, the formation of $BaMnO_{3-\epsilon}$ is never observed. Iodometric titration indicates that the oxygen stoichiometry is close to O_6.

The ordered, oxygen-deficient tetragonal perovskite $LaBaMn_2O_5$ was also prepared by mixing the oxides La_2O_3 and MnO_2 with the carbonate $BaCO_3$, in stoichiometric proportions. But after a preliminary decarbonation at 900 °C, the powders were sintered at 1500 °C in a pure argon flow to avoid any oxydization of Mn^{3+} into Mn^{4+}. The products were then slowly cooled in the same atmosphere to room temperature. Using these conditions, an oxygen-deficient perovskite of the formula

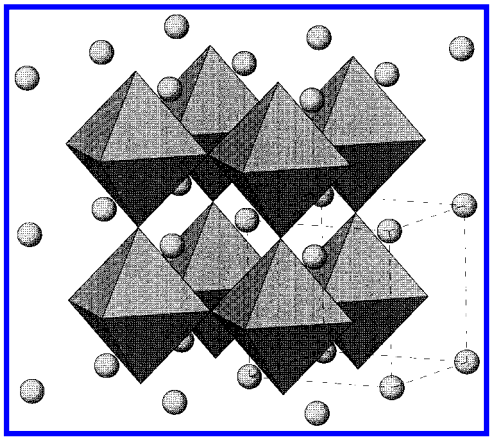

Figure 4. Structure of the disordered perovskite $LaBaMn_2O_6$.

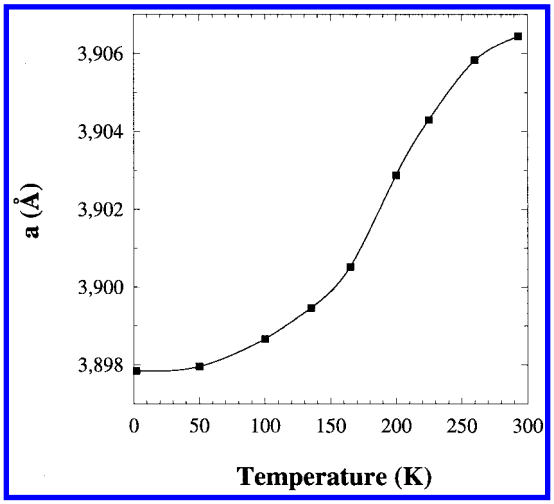

Figure 5. Evolution of the cell parameter and the magnetic moment versus temperature for the disordered perovskite $LaBaMn_2O_6$.

$LaBaMn_2O_{5+\epsilon}$ was obtained with a very small oxygen excess (ϵ) with respect to the ideal formula, O_5. Removal of this excess oxygen was achieved by annealing the obtained powder at 600 °C in an evacuated silica ampule in the presence of zirconium−titanium alloy chips for 12 h. The oxygen content of the sample was then determined by iodometric titration and was found to be very close to the ideal stoichiometry, O_5.

To isolate the ordered stoichiometric tetragonal perovskite $LaBaMn_2O_6$, we annealed the ordered, oxygen-deficient phase at low temperature in the presence of oxygen. Thermogravimetric analysis (Figure 1) revealed that the oxidization begins at very low temperature, ~210 °C; finishs near 230 °C; and occurs in a single step. The weight gain of the thus-obtained sample determined from the TG analysis clearly shows that the oxygen content is close to O_6. It is worth pointing out that the oxygen content of all of these perovskites was further confirmed by the neutron diffraction refinements.

3.2. Nuclear and Magnetic Structure of the Perovskites $LaBaMn_2O_6$ and $LaBaMn_2O_5$

3.2.1. The Disordered Cubic Perovskite $LaBaMn_2O_6$. Both the reconstruction of reciprocal space from the selected area electron diffraction (SAED) patterns and the convergent beam electron diffraction studies for the cubic form of $LaBaMn_2O_6$ confirmed the absence of reflection conditions (Figure 2) and lead to the space group $Pm3m$, with $a = a_P$; [111] and [100] zero-order Laue zone (ZOLZ) CBED patterns show $3m$ and $4mm$ two-dimensional symmetry, respectively.[16−18] The quality of the CBED patterns, even at room temperature, indicates good crystallinity of the samples, which is also confirmed by the evenness of the contrast in the HREM images.

The refinement of this structure was first undertaken in the paramagnetic domain using the room-temperature neutron diffraction data. All of the observed diffraction peaks could be indexed in the space group $Pm3m$ with the unit cell parameter $a_P = 3.9065$ Å. The observed, calculated, and difference profiles are plotted in Figure 3. The refinement converges to give an agreement factor $R_{wp} = 7.41\%$ and $\chi^2 = 1.66$. The cubic symmetry is in agreement with the complete disordering of lanthanum and barium on the same site of the perovskite cell (Figure 4). The evolution of the lattice parameter versus temperature is shown in Figure 5. At room temperature, one observes a Mn−O distance of 1.953 Å which is in agreement with the ionic radii of the Mn^{3+}/Mn^{4+} (1:1) and O^{2-} ions. The neutron diffraction data collected at various temperatures show a ferromagnetic contribution. At 1.7 K, the Mn moment is almost 3.5 μ_B, i.e., exactly the expected spin value for the Mn^{3+}/Mn^{4+} ratio (1:1).

3.2.2. The Ordered, Oxygen-Deficient Tetragonal Perovskite $LaBaMn_2O_5$. For the ordered, oxygen-deficient perovskite $LaBaMn_2O_5$, ED observations on more than 20 crystals showed the existence of extra reflections indicative of the supercell $a_p\sqrt{2} \times a_p\sqrt{2} \times 2a_p$, with the reflection conditions hk0, $h + k = 2n$; $h0l$, none; and hhl, none (Figure 6). In the ED pattern of the latter zone, i.e., $[100]_p$ diffraction, it is the observation of a high-order Laue zone (HOLZ) that confirms the doubling of the cell volume: the first-order Laue zone (FOLZ) is translated by $^1/_2a_p^*$ as compared to the zero-order Laue zone (ZOLZ) reflections, and the measurement of the FOLZ diameter allows evaluation of the reciprocal perpendicular distance between the FOLZ and the ZOLZ as closed to $^1/_2a_p$ Å^{-1}. From the ED investigations, the deduced space group is $P4/nmm$.

While the iodometric titration results indicate the oxygen content to be near O_5, the ED investigations show that complete deoxygenation is not always reached. Indeed, a few crystals have different ED patterns from that discussed above. Two distinct kinds of microcrystals have been characterized. In the first type, $[001]_P$ ED patterns show starlike reflections and associated microdiffraction observations, as well as reciprocal reconstruction, leading to an $a_p \times a_p \times 2a_p$ cell (Figure 7). The corresponding dark-field [001] image shows a tweed-like contrast. Such a phenomenon could be interpreted as microdomains having different oxygen contents close to $O_{5+\epsilon}$. In the second type, the ED patterns show very weak extra spots which index to an

(16) Buxton, B. F.; Eades, J. A.; Steeds, J. W.; Rackham, G. M. *Philos. Trans. R. Soc. London* **1976**, *281*, 171.
(17) Tanaka, M.; Saito, R.; Sekii, H. *Acta Crystallogr.* **1983**, *A39*, 357.
(18) Mornirolli, J. P.; Steeds, J. W. *Ultramicroscopy* **1992**, *45*, 219.
(19) Caignaert, V.; Millange, F.; Domenges, B.; Suard, E.; Raveau, B. (to be published).

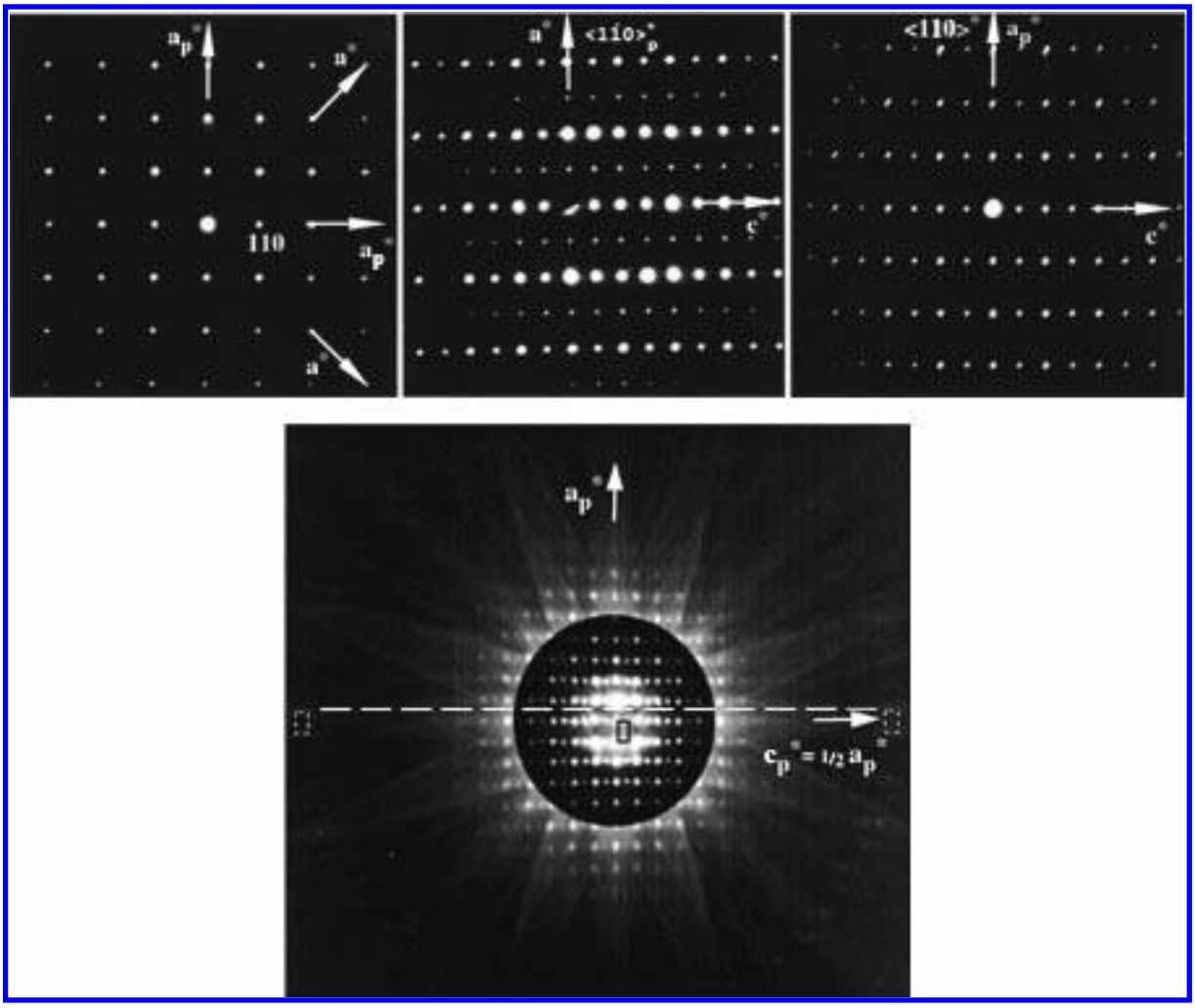

Figure 6. [001], [010], and [110] SAED patterns index to an $a_p\sqrt{2} \times a_p\sqrt{2} \times 2a_p$ cell and show reflection conditions $hk0$, $h + k = 2n$; $h0l$, none; and hhl, none. The [110] microdiffraction shows the doubling of the cell by translation of the FOLZ with respect to the HOLZ; the two-dimensional reciprocal array is materialized through a black rectangle in both the HOLZ and the FOLZ.

$a_p \times 2a_p \times 4a_p$ supercell (Figure 8), similar to that of the partially deoxygenized compound $LaBaMn_2O_{5.5}$.[19] This superstructure effect is not always as well established. In Figure 8b, the SAED pattern only shows a splitting of dots in parallel to the [110]* direction indicative of the coexistence of domains showing a slightly distorted framework. The corresponding HREM image shows a [110] typical $LaBaMn_2O_5$ contrast ($a_p \times 2a_p$ periodicity), but some domains can be distinguished which show modulation of contrast typical of $LaBaMn_2O_{5.5}$ structure ($2a_p \times 4a_p$ centered periodicity). The $b/2$ parameter of the $LaBaMn_2O_{5.5}$ structure and the d_{110} distance of the $LaBaMn_2O_5$ structure being close to 4.09 and 3.99 Å, respectively, this phenomemon is probably responsible for the dot splitting on the SAED pattern. These observations suggest that deoxygenation in a few crystals is only partially achieved, but nonetheless would occur in an ordered fashion (as deduced from synthesis conditions of $LaBaMn_2O_{5.5}$ compound).[19]

The powder neutron diffraction pattern of this phase, collected at room temperature in the paramagnetic domain, was indexed with a tetragonal cell, space group $P4/nmm$ with $a = 5.6501$ Å and $c = 7.8083$ Å, in agreement with the ED results. The data were first analyzed with a "whole pattern fitting" algorithm to determine accurately the profile shape function, background, and cell parameters. This prelimmary study provided good estimates of R_{wp} and χ^2 that could be reached during the structure refinement. This whole pattern fitting led to $R_{wp} = 8.98\%$ and $\chi^2 = 2.25$. One hundred and two Bragg peaks were used to refine 5 positional parameters and 5 isotropic temperature factors. The refinement converged to give an agreement factor $R_{wp} = 10.0\%$ and $\chi^2 = 2.82$. An impurity was identified as MnO and represented less than 1% of the mass of the sample. The observed, calculated, and difference profiles are plotted in Figure 3. Because the ionic radii of La^{3+} and Ba^{2+} are not too different, it is possible to have a statistical occupation of the same site by these two cations. However, refinement of the site occupancies showed that the 2b site is fully occupied by La^{3+} cations (in the oxygen deficient layer), while the 2a site is fully occupied by Ba^{2+} cations.

The structure of $LaBaMn_2O_5$ is quite similar to that of $YBaCuFeO_5$[11,12] or $YBaMn_2O_5$:[13] double layers of apex-sharing MnO_5 pyramids, containing the Ba^{2+} cations, are interleaved with the oxygen-free lanthanum layers. The resultant order of the La^{3+} and Ba^{2+} cations forms layers parallel to (001). The most important difference between the structures of $LaBaMn_2O_5$ and $YBaCuFeO_5$ concerns the ordering of the B-site cations; the existence of two distinct sites for manganese is

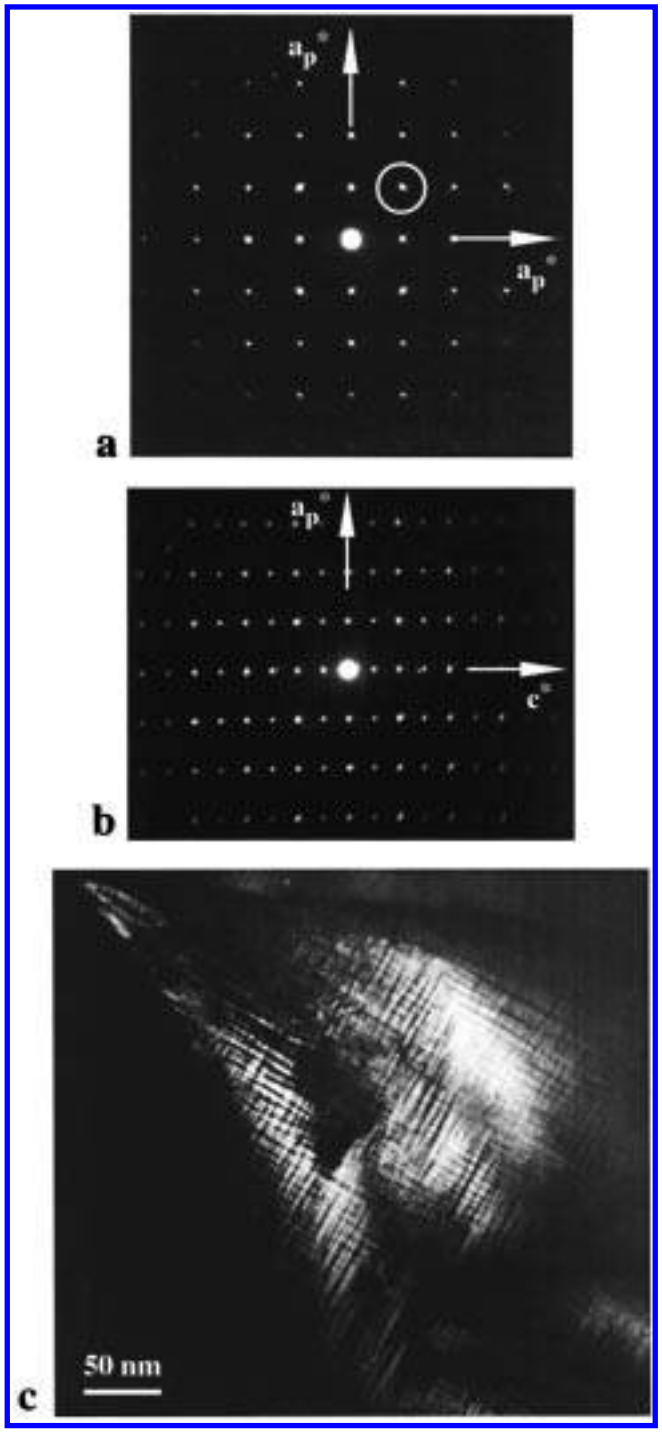

Figure 7. (a, b) [001] and [100] SAED patterns index to an $a_p \times a_p \times 2a_p$ cell. (c) The star-like shape on the [001] SAED pattern is imaged through a tweed-like contrast on a dark-field image obtained from 110 reflection (circled on the SAED pattern).

observed in the former, while the Cu−Fe is of some debate in the latter.[11,12] The final atomic coordinates for $LaBaMn_2O_5$ are listed in Table 1, and the interatomic distances are given in Table 2. The Mn1 and Mn2 sites exhibit average Mn−O distances of 1.965 Å and 2.079 Å, respectively. Taking into consideration the ionic radii of Mn^{3+} and Mn^{2+} ions, it can be assumed that the Mn1 sites are occupied by Mn^{3+} ions and that the Mn2 sites are occupied by the Mn^{2+} ions. Each $Mn^{2+}O_5$ pyramid is linked to five $Mn^{3+}O_5$ pyramids (Figure 9). For the pyramidally coordinated Mn^{3+}, considering the Mn−O bond lengths (four equatorial Mn1−O1 distances of 1.949 Å and one apical Mn1−O2 distance of 2.027 Å), the occupied d_z^2 orbital extends along [001], whereas the unoccupied $d_{x^2-y^2}$ orbital extends along [110] and [1$\bar{1}$0]. Considering the Mn−O bond lengths of the Mn2 site, an orbital order similar to that of the Mn1 site can be assumed for this site, but both the d_z^2 and the $d_{x^2-y^2}$ orbitals are occupied for the high-spin Mn^{2+} cation.

A comparison between the low- and room-temperature neutron diffraction data **(**Figure 10**)** reveals an increase of the intensity of several reflections. These reflections can be indexed on the basis of the nuclear cell, i.e., the magnetic unit cell is $a_p\sqrt{2} \times a_p\sqrt{2} \times 2a_p$. These magnetic peaks correspond to hkl with $h + k = 2n + 1$ and l odd. The first extinction condition implies an antiparallel orientation of the spins within the (a_P,a_P) plane. The second extinction condition implies that, along the *c*-axis, two magnetic atoms separed by *c*/2 have antiparallel magnetic moments. This leads to a G-type antiferromagnetic model (Figure 11). The spin of the magnetic ions is parallel to the *c*-axis (R_{mag} = 5.96%; $\chi^2 = 2.93$ at $T = 1.5$ K). The magnetic moments of the two sites are 2.7(1) μ_B for Mn1 and 3.2(1) μ_B for Mn2. Each Mn^{2+} cation is linked via a Mn−O−Mn bridge to five Mn^{3+} cations, and vice versa. Thus, the order is ferrimagnetic as observed by the susceptibility measurement.

If one considers the Goodenough−Kanamori rules[20] for magnetic interactions in manganese oxides, the expected magnetic order would be A-type. This arises from superexchange interactions between occupied $d_{x^2-y^2}$ orbitals on the Mn^{2+} site with empty $d_{x^2-y^2}$ orbitals on the Mn^{3+} site. Owing to the charge order, each Mn^{2+} site has four Mn^{3+} neighbors in the plane leading to an expected ferromagnetic layer. The interactions between the occupied d_z^2 orbitals in the *c*-direction should be, as observed experimentally, antiferromagnetic. However, as discussed above, the in-plane interactions are also antiferromagnetic, despite the ferromagnetic expectations. This is most likely due to a large distortion of the Mn−O−Mn angles away from the ideal 180° interactions assumed in the Goodenough−Kanamori scenario. This distortion can strongly influence the magnetic interactions, and it is evidently large enough to drive the expected ferromagnetic interactions to become antiferromagnetic; thus, the resultant G-type structure.

3.2.3. The Ordered Stoichiometric Tetragonal Perovskite $LaBaMn_2O_6$. The ED study of the ordered stoichiometric perovskite $LaBaMn_2O_6$ shows that it has tetragonal symmetry with the cell parameters $a_P \times a_P \times 2a_P$. It can be noticed that the extra spots which imply the doubling of the a_p parameter along the *c*-direction are very weak. As will be shown from the structure determination, this observation is not surprising since the cell doubling is only due to La−Ba order and involves almost no distortion of the oxygen framework. This leads to a *c*/*a* ratio, for the ordered phase, of almost exactly 2, and therefore, 90° oriented domain phenomena are very often observed (Figure 12).

For the refinement of the ND data of this compound, we started from the hypothesis that the cation ordering

(20) Goodenough, J. B. *Magnetism and Chemical Bond*; Interscience Publishers: New York, 1966.

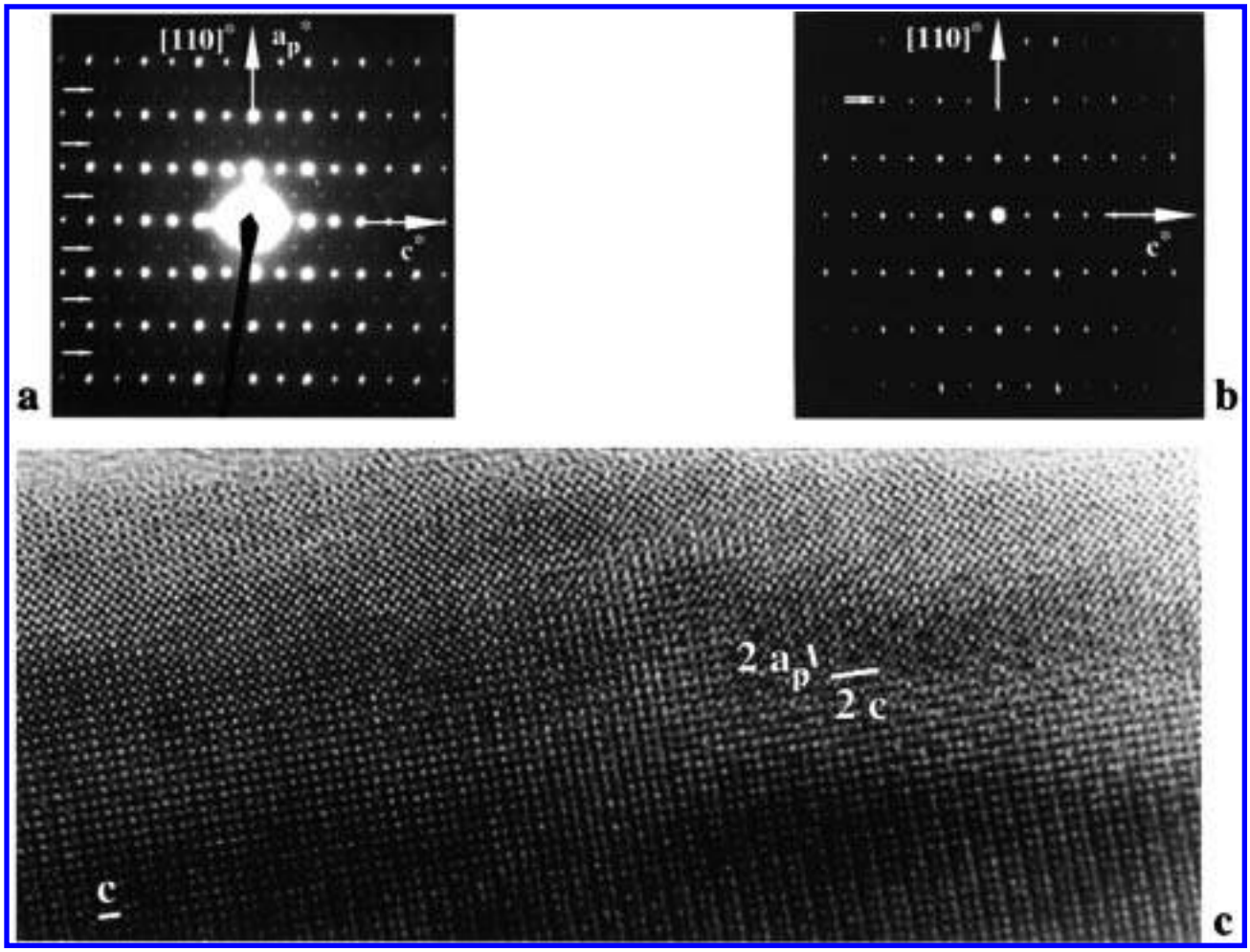

Figure 8. (a) $\langle 100 \rangle_p$ SAED pattern showing weak extra dots which index to the centered two-dimensional array $2a_p \times 4a_p$ similar to the [100] ED pattern of $LaBaMn_2O_{5.5}$ compound. (b) $\langle 110 \rangle$ SAED pattern showing a splitting of dots parallel to the [110]* direction. (c) Corresponding HREM image showing contrast-modulated domains.

Table 1. Refined Structural Parameters of Ordered $LaBaMn_2O_5$ (Space Group *P4nmm*)

		$T = 1.5$ K	$T = 293$ K
La	2b	B_{iso}[a] = 0.22(9)	$B_{iso} = 0.41(9)$
Ba	2a	$B_{iso} = 0.21(9)$	$B_{iso} = 0.45(9)$
$Mn1 = Mn^{III}$	2c	$z = 0.2637(9)$	$z = 0.2632(9)$
		$B_{iso} = 0.46(9)$	$B_{iso} = 0.59(9)$
$Mn2 = Mn^{II}$	2c	$z = -0.2489(9)$	$z = -0.2495(9)$
		$B_{iso} = 0.46(9)$	$B_{iso} = 0.59(9)$
O1	8j	$x = 0.4908(6)$	$x = 0.4913(6)$
		$z = 0.2999(3)$	$z = 0.3002(3)$
		$B_{iso} = 0.60(7)$	$B_{iso} = 0.95(9)$
O2	2c	$z = 0.0061(9)$	$z = 0.0035(9)$
		$B_{iso} = 0.96(9)$	$B_{iso} = 1.09(9)$
a (Å)		5.6386(2)	5.6501(2)
c (Å)		7.7799(4)	7.8083(4)
μ_B	Mn1	2.7(1)	
	Mn2	3.2(1)	
R_p		7.58%	8.26%
R_{wp}		9.02%	10.0%
χ^2		2.93	2.82

[a] Å^2.

Table 2. Selected Interatomic Distances and Angles of Ordered $LaBaMn_2O_5$

	$T = 1.5$ K	$T = 293$ K	multiplicity
La−O1 (Å)	2.530(3)	2.536(3)	×8
Ba−O1 (Å)	3.070(3)	3.081(3)	×8
Ba−O2 (Å)	2.820	2.825	×4
Mn1−O1 (Å)	1.941(4)	1.949(4)	×4
Mn1−O2 (Å)	2.004(9)	2.027(9)	×1
Mn2−O1 (Å)	2.105(5)	2.105(5)	×4
Mn2−O2 (Å)	1.985(9)	1.976(9)	×1
Mn1−O1−Mn2 (deg)	160.8(6)	160.6(8)	
Mn1−O2−Mn2 (deg)	180	180	

observed in the parent phase $LaBaMn_2O_5$ is not strongly affected, because the oxidization is performed at low temperature. Then, the additional oxygen (with respect to O_5) was distributed on the parent phase vacant second apical site (in the lanthanum layer), to transform the MnO_5 pyramids of $LaBaMn_2O_5$ into MnO_6 octahedra for $LaBaMn_2O_6$. The neutron diffraction data at 400 K were first analyzed with a whole pattern fitting algorithm. All of the observed diffraction peaks could be indexed in the space group $P4/mmm$ with unit cell parameters $a = 3.9160$ Å and $c = 7.8054$ Å. This prelimary fit converged to $R_{wp} = 6.47\%$ and $\chi^2 = 1.61$; which could be reached during the final structure refinement. The refinement converged to give an agreement factor $R_{wp} = 7.30\%$ and $\chi^2 = 2.06$. The observed, calculated, and difference profiles are plotted in Figure 3. The final atomic coordinates are listed in Table 3, and the interatomic distances are given in Table 4. These results clearly establish that the structure of the ordered stoichiometric $LaBaMn_2O_6$ perovskite (Figure 13) consists of a pure octahedral $[MnO_3]$ framework, wherein the layered order of the La^{3+} and Ba^{2+} cations along the c-axis of the parent-phase $LaBaMn_2O_5$ is

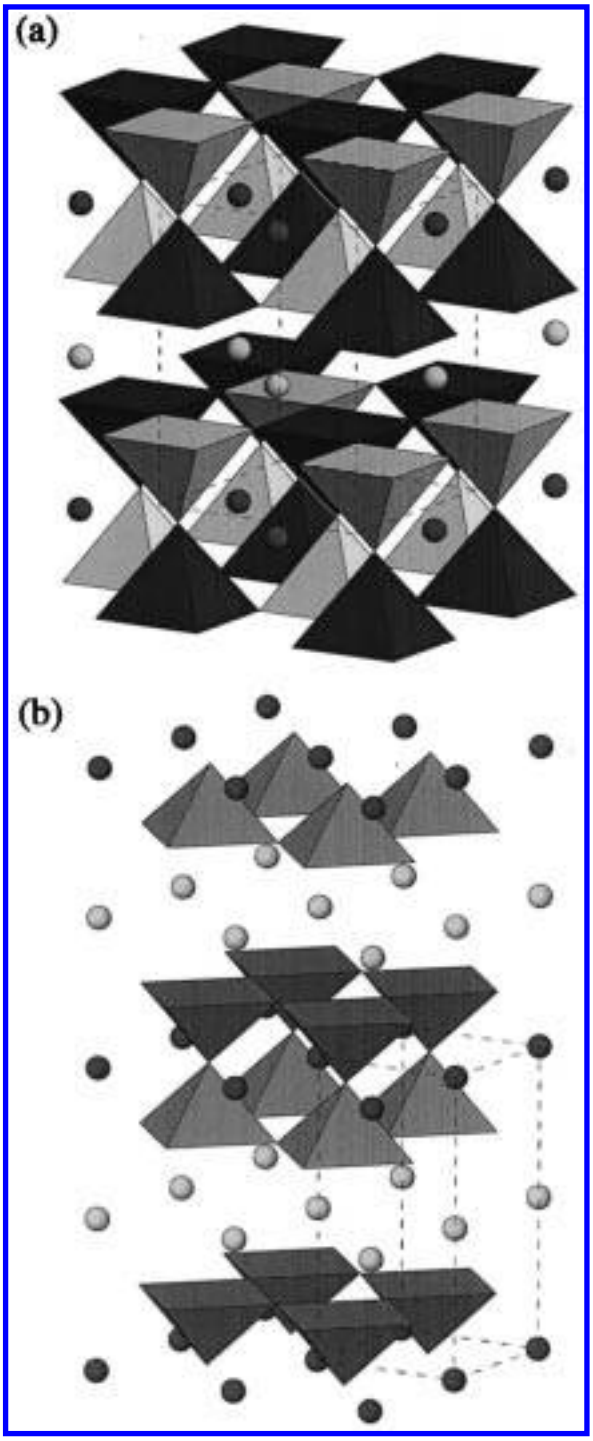

Figure 9. Structure of the perovskites $LaBaMn_2O_5$ (a) and $YBaCuFeO_5$ (b).

preserved. As seen for the cubic-phase $LaBaMn_2O_6$, one observes a ferromagnetic contribution to the powder neutron diffraction data registered at 1.7 K; in contrast to the disordered phase, ferromagnetic contributions are also observed for the room-temperature data of the ordered stoichiometric phase.

3.3. Magnetic and Transport Properties

$LaBaMn_2O_5$, owing to its Mn(II)−Mn(III) mixed valence state and to the order of its Mn(III) and Mn(II) species, exhibits very different magnetic properties from the $LaBaMn_2O_6$ perovskites. The AC and DC susceptibility measurements (Figure 14) are easily explained by considering the Mn(II)/Mn(III) order. One observes a magnetic transition at 100 K, and a ferromagnetic component is clearly revealed by the peak in the imaginary part of the susceptibility. However, the saturated moment obtained from the DC measurement at 5 K is only 0.35 μ_B/Mn (i.e., 0.7 μ_B per $LaBaMn_2O_5$ formula unit), which can be compared to the total moment of 4.5 μ_B/Mn (i.e., 9 μ_B per $LaBaMn_2O_5$) that would result from a ferromagnetically ordered array of $S = {}^5/_2Mn^{2+}$ and $S = {}^4/_2Mn^{3+}$ spins. The neutron results

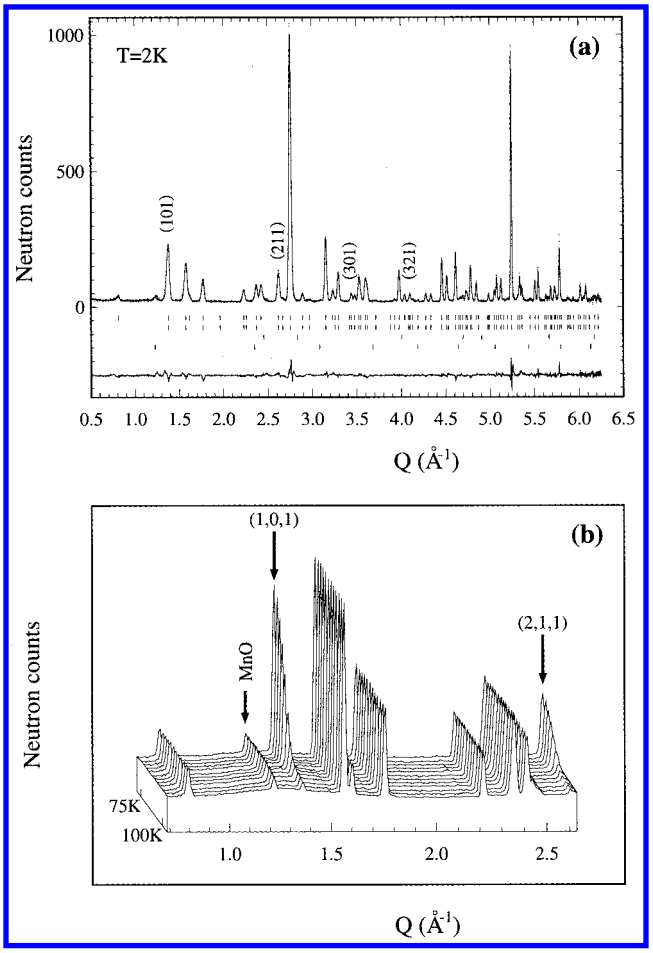

Figure 10. (a) Rietveld refinement plot at 2 K of the neutron diffraction data of the ordered perovskite $LaBaMn_2O_5$. (b) Thermal dependence of the magnetic structure in the temperature range 70−100 K.

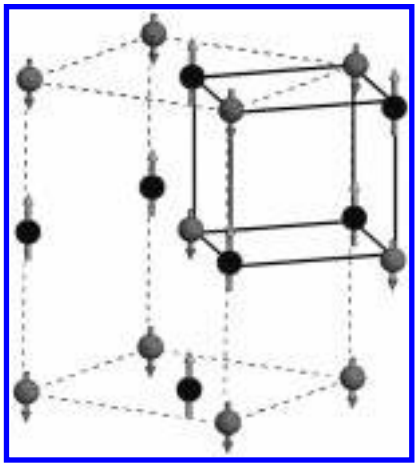

Figure 11. G-type structure of the perovskite $LaBaMn_2O_5$.

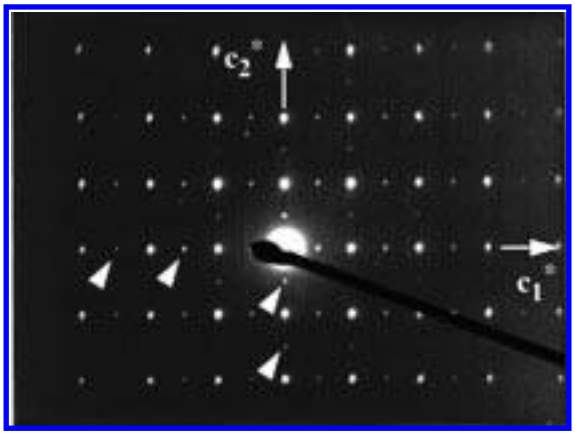

Figure 12. ⟨100⟩ SAED pattern typical of the ordered perovskite $LaBaMn_2O_6$. Two 90° oriented domains can be distinguished. Dots introducing the doubling of the a_p parameter along the *c*-direction (arrowheads) are rather weak compared to the a_p subcell array.

Table 3. Refined Structural Parameters of Ordered $LaBaMn_2O_6$ (Space Group *P4mmm*)

		$T = 1.5$ K	$T = 293$ K	$T = 400$ K
La	1b	B_{iso}[a] = 0.41(9)	$B_{iso} = 0.65(9)$	$B_{iso} = 0.71(9)$
Ba	1a	$B_{iso} = 0.29(9)$	$B_{iso} = 0.51(9)$	$B_{iso} = 0.94(9)$
Mn	2h	$z = 0.2528(9)$	$z = 0.2519(9)$	$z = 0.2514(9)$
		$B_{iso} = 0.33(9)$	$B_{iso} = 0.48(9)$	$B_{iso} = 0.53(9)$
O1	4i	$z = 0.2655(6)$	$z = 0.2649(6)$	$z = 0.2645(6)$
		$B_{iso} = 0.38(9)$	$B_{iso} = 0.94(9)$	$B_{iso} = 1.21(9)$
O2	1c	$B_{iso} = 1.14(9)$	$B_{iso} = 1.52(9)$	$B_{iso} = 1.60(9)$
O3	1d	$B_{iso} = 1.11(9)$	$B_{iso} = 1.34(9)$	$B_{iso} = 1.80(9)$
a (Å)		3.9018(1)	3.9090(1)	3.9160(1)
c (Å)		7.7919(2)	7.7958(2)	7.8054(2)
μ_B		2.879(4)	1.287(5)	
R_p		7.77%	6.72%	5.61%
R_{wp}		11.2%	8.93%	7.30%
χ^2		4.62	1.46	2.06

[a] Å^2.

Table 4. Selected Interatomic Distances and Angles of Ordered $LaBaMn_2O_6$

	$T = 1.5$ K	$T = 293$ K	$T = 400$ K	multiplicity
La−O1 (Å)	2.673(2)	2.679(1)	2.686(1)	×8
La−O3 (Å)	2.759	2.764	2.769	×4
Ba−O1 (Å)	2.843(1)	2.844(1)	2.845(1)	×8
Ba−O2 (Å)	2.759	2.764	2.769	×4
Mn−O1 (Å)	1.953(1)	1.957(1)	1.961(1)	×4
Mn−O2 (Å)	1.970(5)	1.964(4)	1.962(3)	×1
Mn−O3 (Å)	1.926(5)	1.934(4)	1.940(3)	×1
Mn−O1−Mn (deg)	174.19(1)	174.06(1)	174.04(1)	
Mn−O2−Mn (deg)	180	180	180	
Mn−O3−Mn (deg)	180	180	180	

show that the order is ferrimagnetic, with a small ferromagnetic component due to the incomplete compensation of antiferromagnetically ordered sublattices.[13] If all of the $S = {}^5/_2Mn^{2+}$ spins are antiparallel to the $S = {}^4/_2Mn^{3+}$ spins, a saturated moment of 1 μ_B per $LaBaMn_2O_5$ formula unit is expected. This is consistent with the observed value of 0.7 μ_B. As expected from the observed ordered arrangement of the Mn^{2+}/Mn^{3+} species, $LaBaMn_2O_5$ is an insulator.

In contrast to the oxygen-deficient perovskite $LaBaMn_2O_5$, the two stoichiometric $LaBaMn_2O_6$ perovskites are metallic at low temperature. In fact, the $R(T)$ curves of these oxides registered in a zero magnetic field (Figures 15 and 16) and the $M(T)$ curves registered under 100 G show that both of them exhibit a transition

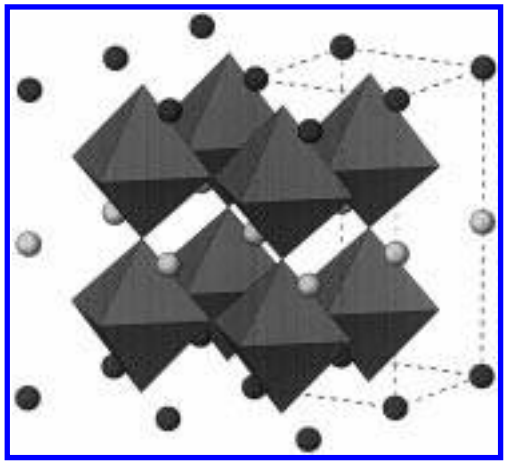

Figure 13. Structure of the ordered perovskite $LaBaMn_2O_6$.

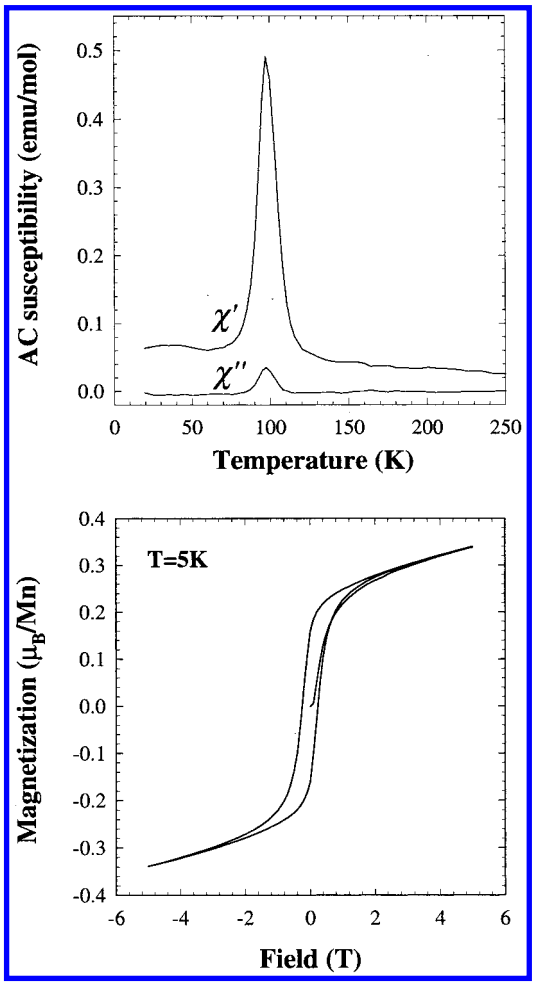

Figure 14. AC and DC susceptibility of $LaBaMn_2O_5$.

from a paramagnetic insulating state to a ferromagnetic metallic state as T decreases. The magnetic moment deduced from the $M(H)$ curves (see Figure 15 (inset) and Figure 16) is 3.5 μ_B at 3.5 K, in agreement with the neutron diffraction data. The behavior of $LaBaMn_2O_6$ can be compared with that of both the insulator $LaMnO_3$ and the CMR manganite $La_{1-x}Ba_xMnO_3$. $LaMnO_3$ is an antiferromagnetic insulator, wherein the antiferromagnetism arises from $Mn^{3+}-O-Mn^{3+}$ superexchange in-

(21) De Gennes, P. G. *Phys. Rev.* **1960**, *118*, 141.

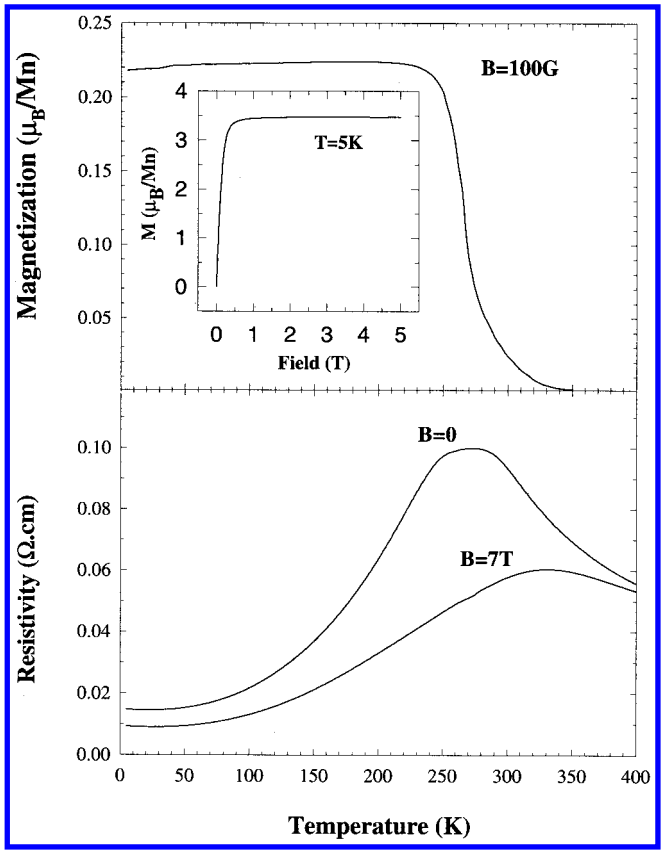

Figure 15. Physical properties of the disordered perovskite $LaBaMn_2O_6$. Top: Magnetisation curve versus T. The inset shows the magnetization curve registered with increasing magnetic field at $T = 5$ K. Bottom: Resistivity curves versus T for $B = 0$ and 7 T.

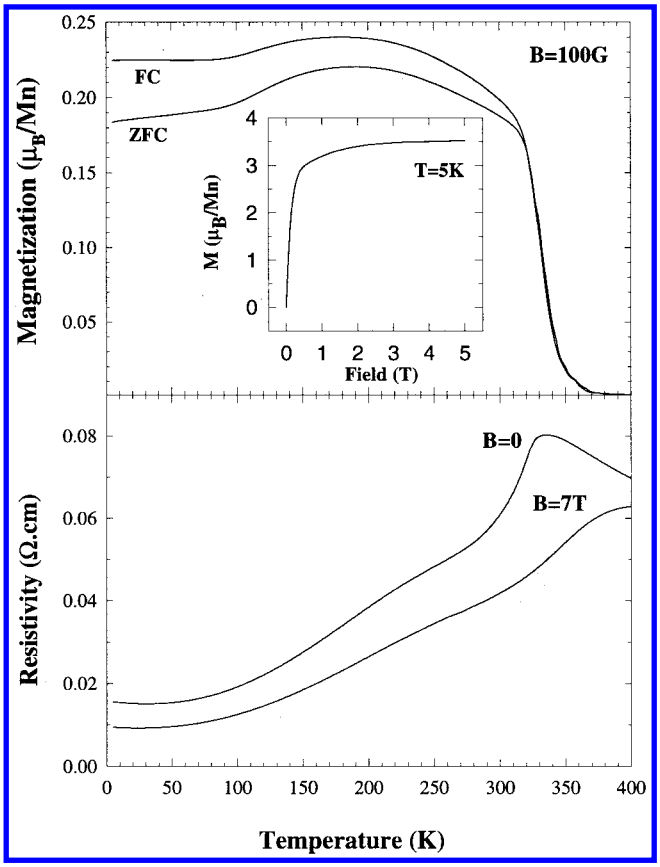

Figure 16. Physical properties of the ordered perovskite $LaBaMn_2O_6$. Top: Magnetization curve versus T. The inset shows the magnetization curve registered with increasing magnetic field at $T = 5$ K. Bottom: Resistivity curves versus T for $B = 0$ and 7 T.

teractions. In $La_{0.5}Ba_{0.5}MnO_3$ (i.e., $LaBaMn_2O_6$), the superexchange is diluted by hole doping: Ba^{2+} substitution on the La^{3+} sites results in a concomitant formation of Mn^{4+} cations. Thus, the magnetic properties of both forms of the O_6 compounds can be understood, to a first approximation, as a result of the double exchange mechanism,[21] leading to a ferromagnetic state at low temperature. As seen in other mixed-valent manganese oxides, a simultaneous transition to a metallic state at T_C (Curie point) leads to a large CMR effect. However, the interesting difference between the two forms of O_6 compounds is that the order on the perovskite A-site lattice plays an important role in determing the value of T_C. T_C is indeed increased from 270 K for the disordered stoichiometric perovskite to 335 K for the ordered perovskite. While the average A-site ionic radius and the mismatch between these radii[8] have been shown to be important chemical considerations in controlling T_C, it is evident that the cationic order also plays an important role. In this case, La/Ba cation order in every other (001) layer leads to an important enhancement of T_C. Since the current compound is the only case where such order is observed, owing to the unique synthetic approach, it is impossible to ascertain completely the effects of this order on the manganese−oxygen interactions which drive the electronic/magnetic properties. Further research on other ordered A-site compounds will undoubtedly yield interesting insights into these chemical and physical phenomena.

4. Concluding Remarks

Using a reducing-type synthesis, we have shown that the x value in the $La_{1-x}Ba_xMnO_3$ system could be increased to $x = 0.5$. Moreover, in a synthetic atmosphere which favors the Mn^{2+}/Mn^{3+} couple, we were able to synthesize the ordered, oxygen-deficient perovskite $LaBaMn_2O_5$. This compound has several unique crystal chemical features, including La/Ba order in every other (001) plane; oxygen vacancies ordered in every La layer; Mn^{2+}/Mn^{3+} order even at room temperature, such that these cations alternate along each direction of the unit cell; and ferrimagnetic order below 100 K. Low-temperature oxidation of this compound leads to an A-cation-ordered oxygen stoichiometric material, $LaBaMn_2O_6$, which differs from the disordered compound directly synthesized in both the cation order and magnetic properties. The T_C of the ordered A-site O_6 compound increases, indicating that cation order plays an important role in directing the electronic/magnetic properties in CMR materials. Coupling between A-site order, oxygen vacancy order, manganese valence state, and orbital order controls the final properties of these materials, and more work is required to elucidate the individual effects of these complex interactions.

Acknowledgment. The authors would like to thank Paul Salvador for helpful discussions.

CM980130V